Mössbauer Investigation of the Photoexcited Spin States and Crystal Structure Analysis of the Spin-Crossover Dinuclear Complex [{Fe(bt)(NCS)$_2$}$_2$bpym] (bt = 2,2′-Bithiazoline, bpym = 2,2′-Bipyrimidine)

Ana B. Gaspar,[a] Vadim Ksenofontov,[b] Sergey Reiman,[b] Philipp Gütlich,*[b] Amber L. Thompson,[c] Andrés E. Goeta,[c] M. Carmen Muñoz,[d] and José A. Real*[a]

Dedicated to the memory of Sergey Reiman

Abstract: The crystal structure of the complex [{Fe(bt)(NCS)$_2$}$_2$bpym] (**1**) (bt = 2,2′-bithiazoline, bpym = 2,2′-bipyrimidine) has been solved at 293, 240, 175 and 30 K. At all four temperatures the crystal remains in the $P\bar{1}$ space group with $a = 8.7601(17)$, $b = 9.450(2)$, $c = 12.089(3)$ Å, $\alpha = 72.77(2)$, $\beta = 79.150(19)$, $\gamma = 66.392(18)°$, $V = 873.1(4)$ Å^3 (data for 293 K structure). The structure consists of centrosymmetric dinuclear units in which each iron(II) atom is coordinated by two NCS$^-$ ions in the *cis* position and two nitrogen atoms of the bridging bpym ligand, with the remaining positions occupied by the peripheral bt ligand. The iron atom is in a severely distorted octahedral FeN$_6$ environment. The average Fe−N bond length of 2.15(9) Å indicates that compound **1** is in the high-

spin state (HS–HS) at 293 K. Crystal structure determinations at 240, 175 and 30 K gave a cell comparable to that seen at 293 K, but reduced in volume. At 30 K, the average Fe−N distance is 1.958(4) Å, showing that the structure is clearly low spin (LS–LS). At 175 K the average Fe−N bond length of 2.052(11) Å suggests that there is an intermediate phase. Mössbauer investigations of the light-induced excited spin state trapping (LIESST) effect ($\lambda = 514$ nm, 25 mW cm^{-2}) in **1** (4.2 K, $H_{ext} = 50$ kOe) show that the excited spin states correspond to the HS–HS and HS–LS pairs.

Keywords: bistability · cooperative effects · dinuclear complexes · iron · photoswitching · spin crossover

The dynamics of the relaxation of the photoexcited states studied at 4.2 K and $H_{ext} = 50$ kOe demonstrate that HS–HS pairs revert with time to both HS–LS and LS–LS configurations. The HS–LS photoexcited pairs relax with time back to the ground LS–LS configuration. Complex [{Fe$_{0.15}$Zn$_{0.85}$(bt)(NCS)$_2$}$_2$bpym] (**2**) exhibits a continuous spin transition centred around 158 K in contrast to the two-step transition observed for **1**. The different spin-crossover behaviour observed for **2** is due to the decrease of cooperativity (intermolecular interactions) imposed by the matrix of Zn^{II} ions. This clearly demonstrates the role of the intermolecular interactions in the stabilization of the HS–LS intermediate state in **1**.

Introduction

The processing of information is based on the ability to control and monitor changes in a particular physical property,

such as the magnetic, optical or electrical response of a functional material. Usually, at the most basic level, only one of these physical variables is used. When two or even three of the different physical properties of the material are

[a] Dr. A. B. Gaspar, Prof. J. A. Real
Institut de Ciència Molecular/Departament de Química Inorgánica
Universitat de València, Edifici de Instituts de Paterna
Apartat de Correus 22085, 46071 València (Spain)
Fax: (+34) 963-544-459
E-mail: jose.a.real@uv.es

[b] Dr. V. Ksenofontov, Dr. S. Reiman, Prof. P. Gütlich
Institut für Anorganische und Analytische Chemie
Johannes Gutenberg Universität
Staudinger Weg 9, 55099 Mainz (Germany)
Fax: (+49) 6131-39-22990
E-mail: guetlich@uni-mainz.de

[c] Dr. A. L. Thompson, Dr. A. E. Goeta
Department of Chemistry, University of Durham
South Road, Durham, DHL 3LE (UK)

[d] Prof. M. C. Muñoz
Departament de Física Aplicada
Universitat Politécnica de València
Camí de Vera s/n, 46022 València (Spain)

Supporting information for this article is available on the WWW under http://www.chemeurj.org or from the author.

simultaneously involved, a new wide range of applications and even new fields of research often appear, such as opto-electronics, magnetooptics and spintronics.[1] The search for molecules or molecular assemblies for information processing is one of the most appealing aims of modern molecular chemistry. Whatever the final goal, a fundamental underlying concept is that of bistability: the ability of the molecular system to adopt two different states at a single temperature.

Spin-crossover (SCO) complexes possess labile electronic configurations, and can be converted between the high-spin (HS) and low-spin (LS) states by variation of temperature and/or pressure and by light irradiation (the light-induced excited spin state trapping (LIESST) effect).[2] In the HS and LS states, spin-crossover compounds reveal differences in magnetism, optical properties, colour and structure. Their magnetic and optical properties may be altered drastically within a narrow range of temperature and/or pressure for cooperative transitions, a characteristic that has made the spin-crossover phenomenon one of the most interesting examples of molecular switching. Many publications underline the potential applications of iron(II) SCO complexes as sensors, and especially in information storage, as molecular switches at the nanoscale level.[3]

The control of the magnetic and optical properties by light remains a challenging topic in materials science in view of the possible implementation within magneto-optical devices. Indeed, several examples of photomagnetic systems in 1) transition-metal coordination compounds,[4a] 2) covalently linked organic polyradicals[4b–e] and 3) organic/inorganic magnetic systems[4f] have already been described. In addition to spin-crossover[2] and valence tautomerism[4a] systems, other photoswitching coordination complexes include Prussian Blue analogues, particularly in which long-range magnetic ordering is modified by light.[5]

Interplay between intramolecular antiferromagnetic coupling and SCO behaviour in the dinuclear complexes [{Fe(L)(NCX)$_2$}$_2$bpym] (L = 2,2′-bipyrimidine (bpym), 2,2′-bithiazoline (bt), 6-methyl-2,2′-bipyridine (CH$_3$-bipy) and X = S, Se) and [{Fe(phdia)(NCS)$_2$}$_2$μ-phdia] has been studied when the systems are perturbed using temperature, pressure or light.[6] A singular feature in these complexes is the presence of a plateau between two separate spin transitions, each one involving about 50% of the iron ions (Figure 1). The spin transition does not begin in both iron centres simultaneously, despite the fact that they have identical surroundings and therefore identical ligand field strengths. Mössbauer spectroscopy in an applied magnetic field has confirmed that the plateau of the spin-transition curve predominantly consists of HS–LS pairs.[6] This result shows that the spin conversion in these dinuclear Fe^{II} systems proceeds through the HS–HS⇌HS–LS⇌LS–LS transformation. The energetic stabilisation of the HS–LS species has been interpreted in terms of a synergy between intra- and intermolecular cooperative interactions (short and long range). This synergy leads to the plateau region in the two-step transition and determines its width.
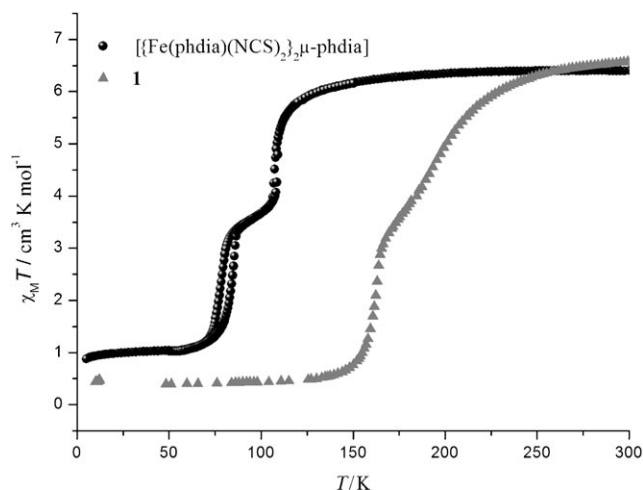

Figure 1. Two-step SCO behaviour for **1** and [{Fe(phdia)(NCS)$_2$}$_2$μ-phdia] systems.

Currently, the question is posed as to whether the two-step behaviour is intrinsic in all dinuclear compounds. In this respect, a gradual transition curve without a plateau has been observed in the [{Fe(dpa)(NCS)$_2$}$_2$bpym] (dpa = 2,2′-di-pyridylamine) derivative; the lack of such a plateau has been ascribed to weak interdimer interactions.[8] A series of new dinuclear iron(II) SCO systems based on pyrazolate and triazolate bridges reported by Murray,[9] Brooker,[10] Kaizaki[11,12] and co-workers has added new interesting results to this topic. The spin conversion in these complexes takes place by means of the HS–HS⇌LS–LS transformation. However, in the case of [{Fe(NCBH$_3$)(4-phpy)$_2$}(μ-bpypz)$_2$]$^{[12]}$ (Hbpypz = 3,5-bis(2-pyridyl)-pyrazol) a two-step transition with 50% HS–HS and 50% LS–LS pairs at the plateau region has been shown by X-ray structure determinations. In bpym- or phdia-bridged dinuclear Fe^{II} compounds, the supposedly predominant factor that determines the existence of the HS–LS species is the strength of the intermolecular interactions in the solid. Indeed, it seems that weak intermolecular interactions are responsible for the direct HS–HS⇌LS–LS transformation in the [{Fe(dpa)-(NCS)$_2$}$_2$bpym]. Moreover, the role of the intermolecular interactions has been demonstrated in the [{Fe(bztpen)}$_2${μ-N(CN)$_2$}][PF$_6$]$_3$·nH$_2$O system, which exhibits a two-step transition in the solid state, while a continuous transition is observed in solution.[13]

Considerable progress has been made in understanding both SCO processes, in spite of the fact that the factors determining the preference of each spin-crossover mechanism have not yet been elucidated. The possibility that similar principles govern the spin-crossover process in which different types of bridging ligands are used cannot be excluded. Recently Murray et al. have found a one-step SCO, HS–HS⇌HS-LS, for the dinuclear complex [Fe$_2$(PMAT)$_2$]-[BF$_4$]$_4$·DMF containing a triazolate bridge.[14] Further experiments in this new kind of dinuclear system are necessary

to explore the importance of the bridging ligand in this context.

On the other hand, it should be stressed that two-step transitions are not associated exclusively with dinuclear systems. There are few well-characterized mononuclear and polymeric systems exhibiting two-step SCO behaviour. The first two step transition was observed for [Fe-(pic)$_3$]Cl$_2$·EtOH[15a] (pic = 2-picolylamine). In this system, long-range ordering interactions inducing spontaneous symmetry breaking and formation of an intermediate phase in which HS and LS molecules coexist in a 1:1 ratio has been observed.[15b] Moreover, this behaviour is also observed in [Fe(btzb)$_3$][PF$_6$]$_2$ (btzb = tris(1,4-bis(tetrazol-1-yl)-butane-N4,N′4).[15b] The occurrence of infinite chains of alternate ···LS–HS–LS··· states has been observed in the plateau displayed by the three-dimensional polymer [Fe-(pmd){Ag(CN)$_2$}{Ag$_2$(CN)$_3$}],[16a] and the presence of inter-layer elastic interactions in the two-dimensional polymer [Fe(H$_3$L^{Me})][Fe(L^{Me})]X (L^{Me} = tris[2-{[(2-methylimidazol-4-yl)-methylidene]amino}ethyl]amine and X = ClO$_4^-$, BF$_4^-$, PF$_6^-$ and AsF$_6^-$) has been shown to produce a HS–LS state in the plateau.[16b]

By irradiation with light of different wavelengths (514 nm, 647.1–676.4 nm) it is possible to photoswitch the HS–HS, HS–LS and LS–LS spin states in the [{Fe(bpym)-(NCSe)$_2$}$_2$bpym] and [{Fe(bt)(NCS)$_2$}$_2$bpym] systems.[6a,c,f,h,i] Furthermore, a selective photoswitching of the HS–HS (λ = 647.1 nm) and HS–LS (λ = 1342 nm) spin states has been reported recently for [{Fe(bt)(NCS)$_2$}$_2$bpym].[7] This selective photomagnetic response of the materials may have relevance to technological applications. Currently, there are certain aspects regarding the photoconversion process of the spin states in the [{Fe(bt)(NCS)$_2$}$_2$bpym] that remain unsolved; for example, whether the discrepancies observed in the percentage of photoinduced species and their nature (HS–HS or HS–LS) can be ascribed to the different wavelength and power of the light used in these experiments. Investigation of the dynamics of the relaxation of metastable spin states also appears to be an important issue. As a continuation of our research in the field of dinuclear SCO systems, we herein report on the nature of the metastable state and the dynamics of its relaxation after the LIESST effect (λ = 514 nm) in the two-step dinuclear SCO complexes [{Fe(bt)-(NCS)$_2$}$_2$bpym] (**1**) and [{Fe$_{0.15}$Zn$_{0.80}$(bt)(NCS)$_2$}$_2$bpym] (**2**). For the first time, the crystal structure characterizations

of **1** in the HS (293 K, 240 K) state, in the LS (30 K) state and in the plateau region of the two-step spin transition (175 K) are reported.

Results and Discussion

Crystal structure determinations for 1: The crystal structure of compound **1** was solved at 293, 240, 175 and 30 K and was found to be in the $P\bar{1}$ space group at all four temperatures. Figure 2 displays the molecular structure of the complex together with the corresponding atomic numbering scheme. Relevant crystal data and selected bond lengths and angles at all four temperatures are presented in Tables 1 and 2, respectively. The structure consists of centrosymmetric dinuclear units in which each iron(II) atom is coordinated by
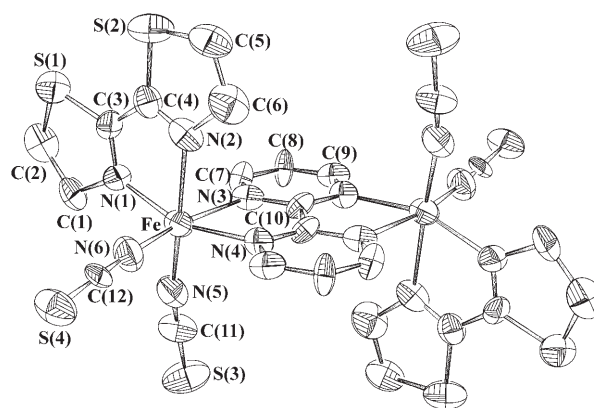

Figure 2. Molecular structure of **1** with the corresponding atom numbering scheme.

Table 1. Crystal data for **1** at different temperatures

	293 K	240 K	175 K	30 K
formula	C$_{24}$H$_{22}$N$_{12}$S$_8$Fe	C$_{24}$H$_{22}$N$_{12}$S$_8$Fe	C$_{24}$H$_{22}$N$_{12}$S$_8$Fe	C$_{24}$H$_{22}$N$_{12}$S$_8$Fe
M_r	846.72	846.72	846.72	846.72
crystal system	triclinic	triclinic	triclinic	triclinic
space group	$P\bar{1}$	$P\bar{1}$	$P\bar{1}$	$P\bar{1}$
a [Å]	8.7601(17)	8.727(4)	8.606(3)	8.434(3)
b [Å]	9.450(2)	9.380(4)	9.271(3)	9.075(3)
c [Å]	12.089(3)	12.096(5)	11.950(4)	11.763(3)
α [°]	72.77(2)	73.052(10)	72.955(7)	72.338(5)
β [°]	79.150(19)	79.508(11)	80.170(7)	80.903(4)
γ [°]	66.392(18)	66.572(12)	67.038(8)	67.617(5)
V [Å^3]	873.1(4)	866.6(7)	837.5(4)	792.3(4)
Z	1	1	1	1
ρ_{calcd} [mg cm^{-3}]	1.610	1.622	1.679	1.775
$F(000)$	430	430	430	430
μ (Mo$_{K\alpha}$) [mm^{-1}]	1.347	1.357	1.404	1.484
crystal size [mm]	0.09 × 0.08 × 0.06	0.14 × 0.12 × 0.08	0.14 × 0.12 × 0.08	0.14 × 0.12 × 0.08
total reflections	3066	4366	4223	2749
reflections [$I > 2\sigma(I)$]	1041	2497	2747	2021
R_1 [$I > 2\sigma(I)$][a]	0.0940	0.0687	0.0646	0.0555
wR	0.1458	0.1474	0.1366	0.1275
S	1.050	1.031	1.023	1.070

[a] $R_1 = \Sigma ||F_o| - |F_c||/\Sigma |F_o|$; $wR = [\Sigma\{w(F_o^2 - F_c^2)^2\}/\Sigma\{w(F_o^2)^2\}]^{1/2}$. $w = 1/[\sigma^2(F_o^2) + (mP)^2 + nP]$ in which $P = (F_o^2 + 2F_c^2)/3$; $m = 0.0207$ (293 K), 0.0574 (240 K), 0.0537 (175 K) and 0.0633 (30 K); $n = 8.5826$ (293 K), 1.1768 (240 K), 1.4408 (175 K) and 1.2173 (30 K).

Table 2. Selected bond lengths [Å] and angles [°] for **1**.

	293 K	240 K	175 K	Contraction 1	30 K	Contraction 2
Fe−N(1)	2.112(12)	2.151(5)	2.058(4)	0.093(8)	1.945(5)	0.112(9)
Fe−N(2)	2.239(12)	2.217(4)	2.087(3)	0.130(7)	1.963(5)	0.124(9)
Fe−N(3)	2.256(11)	2.223(4)	2.106(4)	0.117(8)	1.975(4)	0.131(8)
Fe−N(4)	2.194(13)	2.193(5)	2.089(4)	0.104(8)	1.977(5)	0.112(8)
Fe−N(5)	2.070(14)	2.066(5)	2.011(5)	0.055(8)	1.947(5)	0.064(10)
Fe−N(6)	2.042(13)	2.050(5)	1.981(5)	0.069(8)	1.935(5)	0.046(9)
average Fe−N distance	2.152(11)	2.142(10)	2.052(11)	0.090(15)	1.958(4)	0.094(12)
octahedral volume [Å³]	12.84(11)	12.80(4)	11.35(4)	1.45(6)	9.93(4)	1.42(6)
N(1)-Fe-N(2)		74.65(17)	77.34(15)		80.8(2)	
N(1)-Fe-N(3)		94.61(16)	94.93(15)		95.17(18)	
N(1)-Fe-N(4)		158.82(15)	164.96(14)		172.2(2)	
N(1)-Fe-N(5)		94.9(2)	94.90(17)		94.0(2)	
N(1)-Fe-N(6)		97.58(19)	94.75(17)		90.92(19)	
N(2)-Fe-N(3)		85.20(15)	87.33(14)		90.22(19)	
N(2)-Fe-N(4)		86.07(16)	88.82(14)		91.6(2)	
N(2)-Fe-N(5)		165.21(19)	168.96(17)		173.15(18)	
N(2)-Fe-N(6)		94.48(16)	93.84(15)		92.4(2)	
N(3)-Fe-N(4)		74.77(15)	78.39(14)		82.66(18)	
N(3)-Fe-N(5)		85.25(17)	85.52(15)		85.81(19)	
N(3)-Fe-N(6)		167.26(19)	170.27(17)		173.69(19)	
N(4)-Fe-N(5)		102.25(18)	97.95(16)		93.4(2)	
N(4)-Fe-N(6)		92.50(18)	91.97(16)		91.52(18)	
N(5)-Fe-N(6)		97.31(19)	94.63(17)		92.1(2)	
Fe−Fe···Fe−Fe distances						
intramolecular	5.919(3)	5.890(3)	5.638(2)		5.355(2)	
intrastack	8.570(4)	8.573(3)	8.641(3)		8.632(3)	
bt–bt interaction	8.262(4)	8.267(3)	8.116(3)		7.888(3)	
C−H···S interaction	8.029(4)	8.069(3)	8.182(2)		8.260(3)	
intermolecular contacts						
S1···S4	3.605(7)	3.504(7)	3.564(3)		3.494(3)	
C7−H7···S3	2.837(7)	2.758(4)	2.779(3)		2.748(3)	

two NCS⁻ anions in the *cis* position and two nitrogen atoms of the bridging bpym ligand, with the remaining positions occupied by the peripheral bt ligand. The iron atom is in a severely distorted octahedral FeN_6 environment. The thiocyanate Fe−N bond lengths are noticeably shorter than the other four Fe−N distances: Fe−N(6) = 2.042(13) and Fe−N(5) = 2.070(14) Å, compared with Fe−N(1) = 2.112(12), Fe−N(2) = 2.112(12), Fe−N(3) = 2.256(11) and Fe−N(4) = 2.194(13) Å. The average Fe−N bond length of 2.15(9) Å indicates that at 293 K compound **1** is in the high-spin state, which is in agreement with magnetic and Mössbauer data.[6] The intramolecular Fe···Fe distance across the bpym bridge at this temperature is 5.919(3) Å.

The data collected at 240, 175 and 30 K revealed a cell comparable to that seen at 293 K, but reduced in volume. On cooling to 175 K, there is a unit cell volume contraction of 4%, from 873.1(4) (293 K) to 837.5(4) Å³, suggesting that there is a change in the spin state. On cooling down to 30 K there is a further contraction to 792.3(4) Å³, which corresponds to an additional 5.25% decrease (based on the unit cell at 293 K). The average Fe−N distance at 30 K of 1.958(4) Å indicates that the structure is clearly low spin. However, at 175 K the average Fe−N bond length of 2.052(11) Å is exactly half way between the high- and low-spin values, suggesting that there is an intermediate phase. The data at 175 K was scrutinised for the presence of super

lattice reflections, but none were found. At the plateau, the Mössbauer and magnetic data[6] indicate that the intermediate state is half way between the high- and low-spin states, consisting of HS–LS pairs, which is in keeping with the results for the average bond length. It is more likely therefore, that the HS and LS iron(II) centres are ordered in some way, similar to [Fe(pic)₃]Cl₂·EtOH as discussed by Chernyshov et al.[15b] However, in [Fe(pic)₃]Cl₂·EtOH the super lattice reflections due to the differences between the HS and LS centres were only visible with synchrotron radiation. In the case of compound **1**, a $Mo_{K\alpha}$ X-ray source was used, so it is quite possible that any super lattice reflections, similar to those observed by Kaizaki[12] and co-workers, were invisible. Another possible explanation to justify the lack of broken symmetry in the plateau region could be associated with the fact that the HS–LS species are disordered in the crystal, so that the X-ray diffraction analysis only sees the average structure of the HS and LS centres. The structural changes noted between 293 and 30 K in the Fe^{II} coordination environment for **1** are similar to those reported in references [9–11].

The individual Fe−N distances generally follow a similar pattern on cooling down to 30 K, with the shortest Fe−N distance being that to the thiocyanate ligands, as is commonly observed (Table 2).[2] It is interesting to note, however, that Fe−N(3) is the longest of the remaining four, while Fe−

N(1) is by far the shortest, a situation that is generally true at all temperatures. Fe−N(2) and Fe−N(4) change their relative lengths, with Fe−N(2) longer at 293 and 240 K, shorter at 30 K, and Fe−N(2) and Fe−N(4) identical at 175 K. In other words, at 293 and 240 K, Fe−N(1) ≪ Fe−N(4) < Fe−N(2) < Fe−N(3), while at 175 K Fe−N(1) ≪ Fe−N(4) = Fe−N(2) ≪ Fe−N(3), which changes to Fe−N(1) < Fe−N(2) < Fe−N(4) = Fe−N(3) at 30 K, in which the range is also reduced. Thus Fe−N(2) experiences the largest contraction, followed by Fe−N(3). The intramolecular Fe···Fe distance behaves as would be expected, decreasing regularly as the crystal is cooled and the structure becomes low spin.

There are no conventional hydrogen bonds, but there are weak C−H···S interactions and, in this case, also S···S close contacts. The molecules pack together with bpym rings sitting in stacks along the *a* axis. There are no π–π interactions; the bpym rings are in fact slightly staggered and two of the thiocyanate ligands intrude, ending in a bpym–bpym distance of 8.760 Å at 293 K (Figure 3 top). The thiocyanate ligand points away from the iron centre towards the bpym ligand of the next molecule in the stack, so that the sulfur atom sits between the two rings. In this way, the stacks contain bpym rings alternating with sulfur atoms. This sulfur atom (S(3)), experiences a C−H···S type interaction from one of the hydrogen atoms on the bpym ligand in the adjacent stack, a relationship that is reciprocated. Viewed down the *c* axis an overlap between the bt ligands can also be seen. Since bt is not an aromatic ligand, π–π type interactions are not possible, but the distance between the planes of the overlapping bt ligands at 293 K is 3.93(1) Å. This is probably caused by the weak S···S interaction between one of the bt sulfur atoms (S(1)) and one of the thiocyanate ligands (S(4)), (S(1)···S(4) = 3.605(7) Å, 293 K) (Figure 3 bottom). The rings of the bt ligands are nearly planar with a dihedral angle of 8.4(5)°. A similar overlapping between bt ligands has been observed in the [Fe(bt)$_2$(NCS)$_2$] polymorph A, although in this complex the S···S interactions are between the sulfur atoms of the bt ligands.[17]

In compound **1**, at 293 and 240 K, the shortest interdimer (Fe−Fe···Fe−Fe) distance is determined to be the C(7)−H(7)···S(3) intermolecular contact, being 8.029(4) and 8.069(3) Å, respectively (Table 2). This distance increases by 0.153(5) Å during the first step (293 to 175 K) and by 0.078(5) Å between 175 and 30 K. There are two more short distances (less than 8.5 Å) at 293 K; one is through the bt–bt ligand overlap and the other is the distance between adjacent dimers in the stack along the *c* axis (Figure 4, Table 2). It is worth mentioning that this last distance increases by 0.068(5) Å on cooling from 240 to 175 K, but undergoes almost no further change on cooling to 30 K. In contrast, the interdimer distance through the bt–bt ligand overlap decreases, undergoing changes of 0.151(5) and 0.228(5) Å at 175 and 30 K, respectively.

Photoswitching of spin states monitored by Mössbauer spectroscopy: Figure 5a illustrates the Mössbauer spectrum of **1** at 4.2 K. The sample was enriched with 20% of ^{57}Fe in
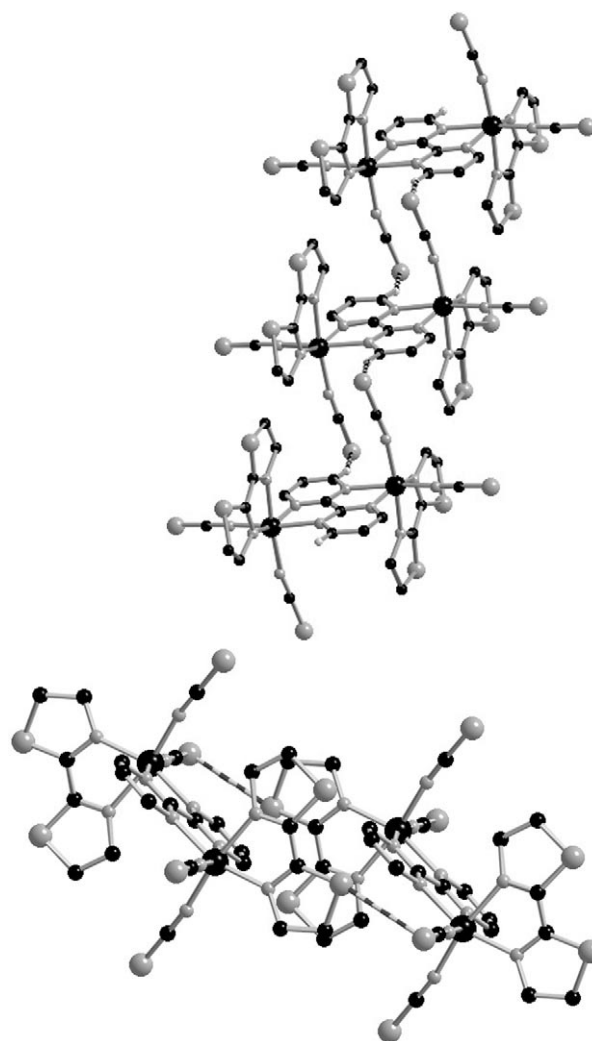

Figure 3. Top: View of the packing and stacking in **1** along the [010] direction. Intermolecular short contacts are observed between the sulfur atoms of the thiocyanate ligands and the hydrogens of the bpym ligands (dotted lines); Bottom: Overlapping between bt ligands of adjacent dimers; intermolecular contacts are denoted by dotted lines.
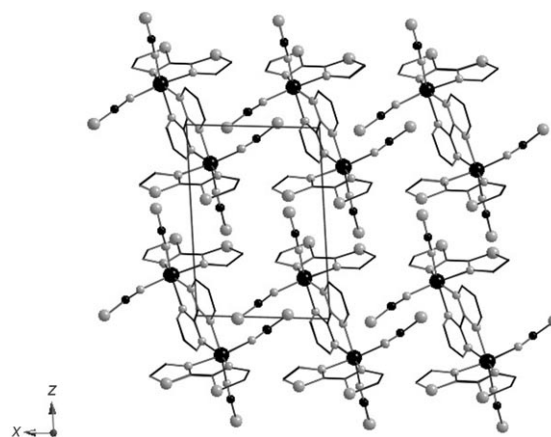

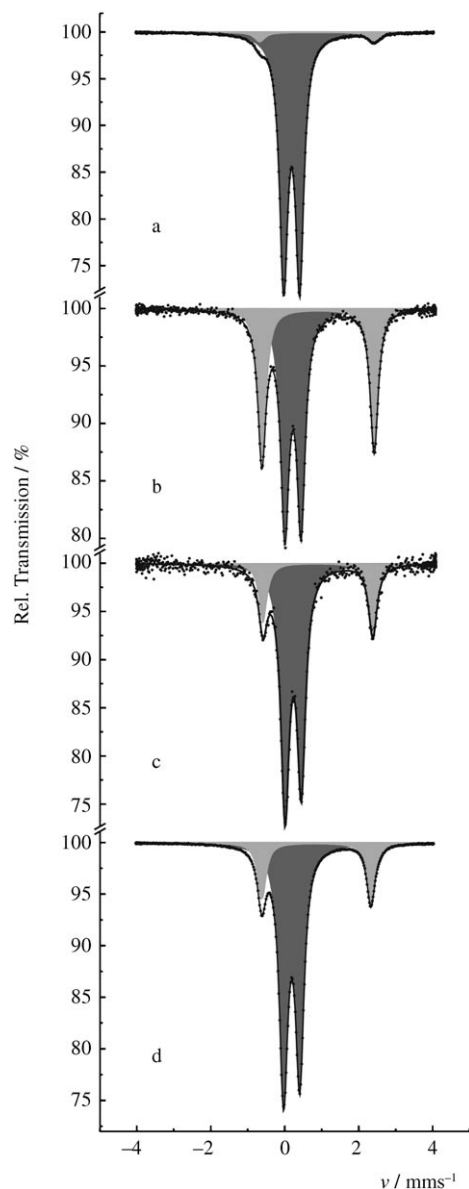Figure 4. View of the crystal packing of **1** along the *c* direction.

Figure 5. ^{57}Fe Mössbauer spectra of **1** recorded at 4.2 K in zero-field a) before irradiation, b) immediately after irradiation, c) six days and d) 11 days after irradiation. Mössbauer subspectra correspond to: HS species (grey), LS species (dark grey).

Figure 6. Time dependence of the fraction of metastable HS molecules, in the form of HS–HS and HS–LS pairs, for **1** after LIESST at 4.2 K.

order to improve the quality of the Mössbauer spectra. The spectrum shows that the LS species is predominate. The Mössbauer parameters obtained from the fitting of the spectrum are: $\delta_{LS} = 0.357(1)$ mm s^{-1}, $\Delta E_{Q(LS)} = 0.452(2)$ mm s^{-1}. After irradiation of the sample for one hour ($\lambda = 514$ nm, 25 mW cm^{-2}) at 4.2 K, the Mössbauer spectrum of **1** shows a decrease in the intensity of the LS species (62 %) in favour of an increase of the HS species (38 %) (Figure 5b). It was confirmed by means of Mössbauer experiments with samples of different thickness that irradiation affected not only the surface, but also the entire bulk of the sample. Time-dependent measurements revealed the decay of the HS component (Figure 5c,d), which reached an asymptotic value of about 20 % within approximately ten days (Figure 6). Möss-
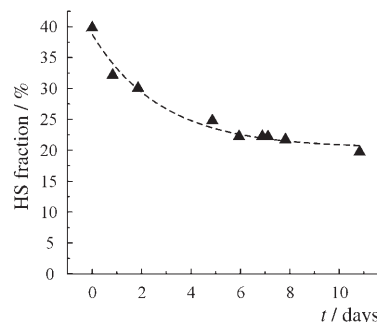
bauer measurements in a magnetic field of 50 kOe at 4.2 K allow the identification of the nature of the metastable states.[6a,f] As shown in Figure 7a the total spectrum measured at 4.2 K and $H_{ext} = 50$ kOe after light irradiation consists of three components. The component with the isomer shift being equal to $\delta_{LS-LS}(\mathbf{1}) = 0.21(1)$ mm s^{-1} and $H_{eff} \approx H_{ext}$ is identified as the "fingerprint" of the LS state. The second low-intensity broadened doublet with parameters $\delta_{HS-HS}(\mathbf{1}) = 0.84(2)$ mm s^{-1}, $\Delta E_{Q(HS-HS)}(\mathbf{1}) = 3.10(3)$ mm s^{-1} and $H_{eff} = 16.7(5)$ kOe, corresponds to iron(II) ions in antiferromagnetically coupled HS–HS pairs. The values for $\delta_{HS-HS}(\mathbf{1})$ and $\Delta E_{Q(HS-HS)}(\mathbf{1})$ are close to the values reported for [{Fe-(bpym)(NCS)$_2$}$_2$bpym], in which the ground spin state corresponds to antiferromagnetically coupled HS–HS pairs.[6f,g] The third component with parameter values $\delta_{HS-LS}(\mathbf{1}) = 0.84(2)$ mm s^{-1} and $\Delta E_{Q(HS-LS)}(\mathbf{1}) = 3.0(1)$ mm s^{-1} is unambiguously assigned to the HS state in HS–LS pairs, because the measured effective magnetic field at the iron nuclei of 85 kOe clearly originates from a spin-quintet ground state of iron(II) ($S = 2$). The values of $\delta_{HS-LS}(\mathbf{1})$, $\Delta E_{Q(HS-LS)}(\mathbf{1})$ and H_{eff} are similar to the values observed for the [{Fe(bpym)-(NCSe)$_2$}$_2$bpym] complex with a paramagnetic HS–LS ($S = 2$) ground state.[6f,g]

The important result of the LIESST experiments in **1** is that the photoinduced species are not only HS–HS but also HS–LS pairs. The appearance of HS–LS species should be interpreted in terms of a synergy between intramolecular and intermolecular cooperative interactions that stabilise the mixed pairs energetically. From the time-dependent area fraction subspectra of the irradiated sample **1** (Figure 7a–d) one can derive the dynamics of the transformation between HS–LS, HS–HS and LS–LS pairs (Figure 8). The time-dependent measurements reveal that HS–HS pairs are unstable and revert with time to both HS–LS and LS–LS configurations. In turn, the HS–LS pairs also relax back to the LS–LS pairs with time.

These findings are in agreement with results from DFT calculations on the energetics of dinuclear spin-transition complexes.[18] The authors have computed the relative energies of the LS–LS, HS–LS and HS–HS pairs for four dinuclear iron(II) complexes of the class [{Fe(L)(NCX)$_2$}$_2$bpym] (L = bpym, bt and X = S, Se), the ground states of which are in order of increasing ligand field strength: HS–HS for
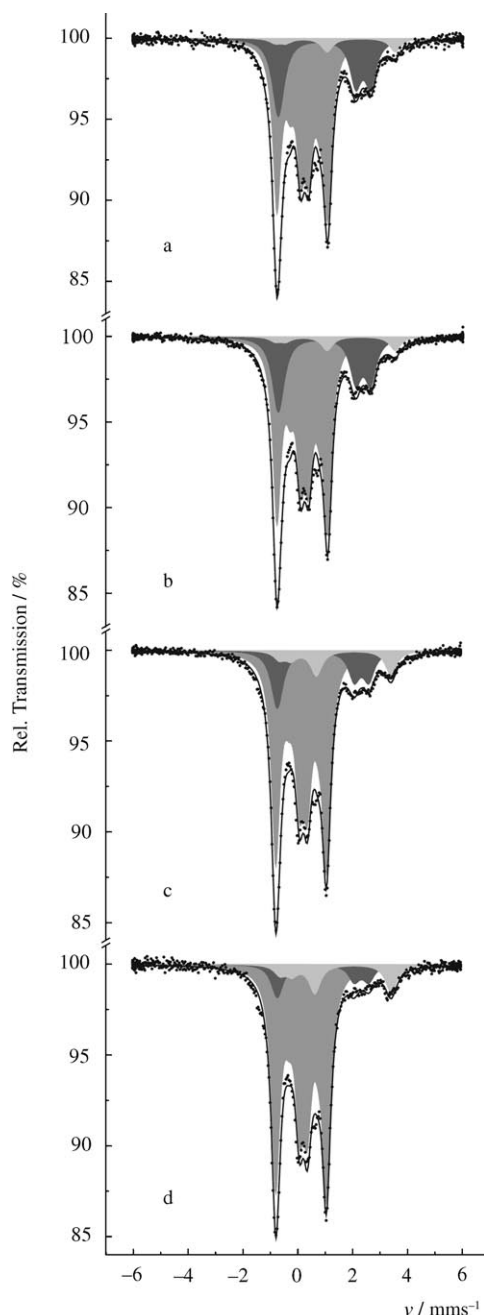
Figure 7. ^{57}Fe Mössbauer spectra of **1** at 4.2 K in a magnetic field of 50 kOe recorded a) one day, b) two days, c) five days and d) six days after light irradiation. LS in HS–LS and LS–LS pairs (grey), HS in HS–LS pairs (light grey), HS in HS–HS pairs (dark grey).

(bpym, S), HS–LS for (bpym, Se), LS–LS for (bt, S), LS–LS for (bt, Se). The last two systems are known to show complete spin transition in two steps from HS–HS via the intermediate mixed state HS–LS to LS–LS. The enthalpies of the HS–LS states in these systems lie below the average energies between the LS–LS and the HS–HS states, which appears to be a prerequisite for the occurrence of a two-step transition with the HS–LS state as an intermediate. The stability of the HS–LS state depends on the ratio of $W/\Delta H$, in
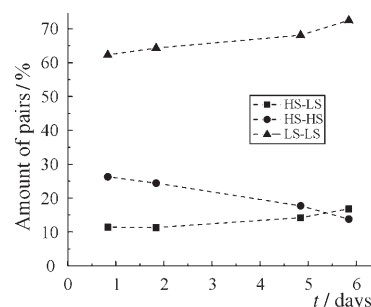

Figure 8. Time dependence of the fraction of different pairs, HS–HS, HS–LS and LS–LS in **1** after LIESST at 4.2 K.

which ΔH is the enthalpy difference between the LS–LS and HS–HS states and W is the difference between the HS–LS enthalpy and the average enthalpies. The larger the value of W, the closer in energy is the HS–LS state to the LS–LS ground state, and therefore the greater the tendency for HS–LS formation during the thermal spin transition. This state is likely to be reached most easily by light irradiation (LIESST). This is in accordance with the present studies of the photoexcited spin states of the dinuclear system (bt, S; **1**). The relative amounts of the different spin-state pairs as shown in Figure 8 are in line with the energetic ordering as calculated by Zein and Borshch for (bt, S; **1**);[18] that is, the HS–LS state lies 12 kJ mol^{-1} above the LS–LS ground state, and the HS–HS state lies 24 kJ mol^{-1} above the intermediate HS–LS state. Accordingly the amount of LS–LS ground state increases and the least stable HS–HS state decreases with time elapsed after irradiation at 4.2 K. It is interesting to note that the HS–HS state relaxes partially to the relatively stable mixed-spin state HS–LS, the relaxation of which to the most stable LS–LS state seems to be kinetically hindered at very low temperatures (4.2 K in the present study).

To investigate in more detail and to prove experimentally the role of the intermolecular interactions in the stabilisation of the intermediate HS–LS state, a solid solution of composition [{Zn$_{0.85}$Fe$_{0.15}$(bt)(NCS)$_2$}$_2$bpym] (**2**) was synthesised (complex [{Zn(bt)(NCS)$_2$}$_2$bpym] and **1** are isostructural, see the Supporting Information). It should be noted here that the formation of the heterometallic dinuclear molecules in this solid solution is almost prevented by the synthetic method employed (see Experimental Section). In fact, Mössbauer spectra recorded at 4.2 K in **2** (cf. below) confirm the presence of mainly LS–LS pairs belonging to [{Fe(bt)(NCS)$_2$}$_2$bpym] dimers. If the heterometallic dimers exist in the solid solution the relative amount would be less than 2%, which corresponds to the detection limit of the Mössbauer spectroscopy technique. Moreover, the magnetic susceptibility measurements in **2** below 50 K match very well with what was observed in the Mössbauer spectra.

The effect of dilution of spin-transition complexes into the lattice of isostructural species that do not or cannot show SCO has proved to be very diagnostic of the function of cooperative interactions in influencing the nature of spin-

crossover solids. If the spin state in a particular metal centre changes from LS to HS, the molecular volume increases by around 3–5%, leading to an expansion of the lattice, which causes a change of the "chemical pressure" acting on all complex molecules in the crystal. This facilitates further spin-state changes in other centres. With decreasing iron concentration in a crystal diluted with zinc, the crystal volume change per iron complex decreases, and thus the chemical pressure also decreases. As a consequence an increasingly gradual (less cooperative) nature of the transition is observed together with a displacement of the transition to lower temperatures.[2d,19]

The thermal dependence of γ_{HS} for **2** and **1** derived from the magnetic susceptibility measurements is depicted in Figure 9 ($\gamma_{HS}=$ HS molar fraction). Compound **2** undergoes
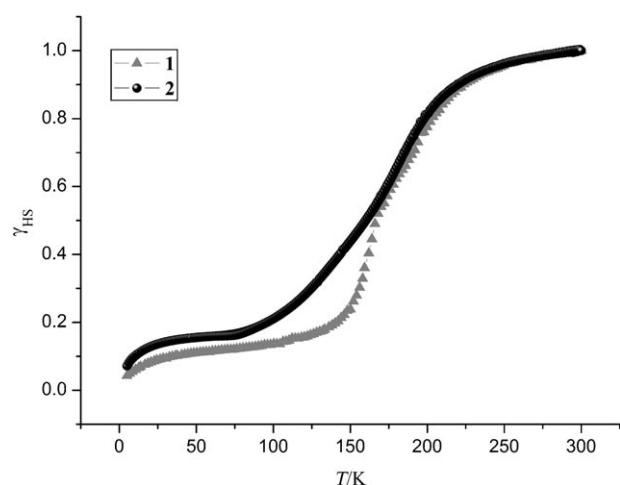
Figure 9. Thermal dependence of the high-spin fraction, γ_{HS} versus T, for **2** and **1** derived from magnetic susceptibility measurements.

an almost complete spin transition with the features of a diluted sample. The beginning of the transition occurs at the same temperature as observed for **1,** but in this case the transition is continuous, no plateau is observed and it is shifted to lower temperatures. The temperature at which $\gamma_{HS}=\gamma_{LS}=0.5$ for **2** is 158 K. As would be expected the cooperativity decreases considerably in **2** compared with **1**. Indeed, the two-step spin transition observed in the neat compound is converted into a continuous transition in the mixed crystal with only 15% iron(II). This clearly demonstrates the role of the intermolecular interactions in the stabilization of the mixed-spin state HS–LS. It should be stressed here that these are the first dilution experiments performed in iron(II) dinuclear complexes.

On the basis of these findings one could expect that only HS–HS pairs would appear as a metastable state after LIESST in compound **2**. The Mössbauer spectrum of compound **2** at 4.2 K is shown in Figure 10a, and the spectrum reflects the presence of the LS species. The Mössbauer parameters obtained from the fitting of the spectrum are: $\delta_{LS}(\mathbf{2})=0.37(1)$ mm s^{-1}, $\Delta E_{Q(LS)}(\mathbf{2})=0.34(2)$ mm s^{-1}. During a

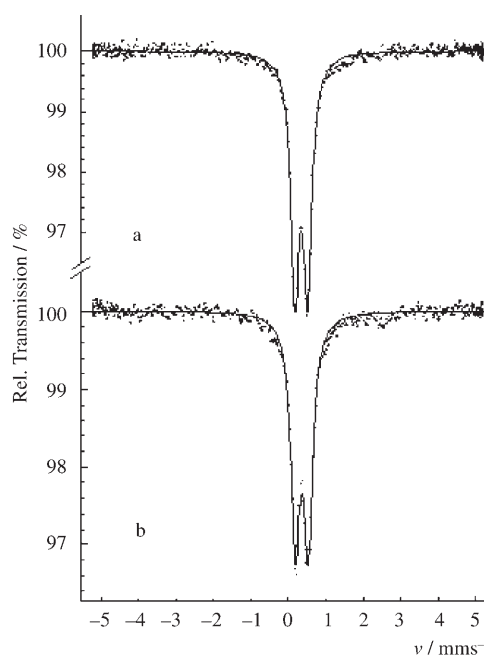Figure 10. ^{57}Fe Mössbauer spectra of [{Zn$_{0.85}$Fe$_{0.15}$(bt)(NCS)$_2$}$_2$bpym] (**2**) recorded at 4.2 K in zero-field a) before irradiation and b) simultaneously with the light irradiation.

continuous irradiation of the sample ($\lambda=514$ nm) at 4.2 K, the simultaneously measured Mössbauer spectrum of **2** does not show any significant traces of the HS species (Figure 10b). Surprisingly, no LIESST effect is observed for **2**. At present we cannot interpret such a result, as further experiments at different wavelengths on matrixes of different composition will be necessary.

Conclusion

In summary, we have shown that the LS–LS ground state of the [{Fe(bt)(NCS)$_2$}$_2$bpym] compound can be partially photoconverted to the HS–HS and HS–LS states by irradiation with $\lambda=514$ nm. The HS–HS metastable spin state relaxes back to the LS–LS ground state through the HS–LS metastable state, the relaxation of which to the most stable LS–LS seems to be kinetically hindered at very low temperatures. Dilution experiments on [{Fe(bt)(NCS)$_2$}$_2$bpym] have proven the role of the intermolecular interactions (short and long range) in the energetic stabilisation of the mixed intermediate HS–LS state characteristic of the two-step spin transition in dinuclear SCO systems.

Experimental Section

FULL PAPER

methanol (25 mL), changing the colour of the solution to violet. A solution of 2,2′-bipyrimidine (bpym) (15 mL) in methanol (0.125 mmol) was added dropwise to this solution. The final dark red solution was filtered and allowed to evaporate for a week, giving prismatic black crystals of **1** suitable for X-ray studies. Yield: 50%; elemental analysis calcd (%) for $C_{24}H_{14}N_{12}S_8Fe_2$: C 34.37, H 1.68, N 20.04; found: C 33.89, H 1.54, N 20.87.

Synthesis of $^{57}FeCl_2·4H_2O$: $^{57}Fe_2O_3$ (100 mg) was dissolved in HCl (80 mL, 37%) and heated at 50°C for 1 hour to facilitate the dissolution of the oxide. Metallic iron powder (600 mg) was added to the resulting yellow solution, and the solution was stirred for one week under a current of argon. After the complete evaporation of the aqueous solution colourless square crystals were obtained. Yield: 90%; elemental analysis calcd (%) for $FeCl_2O_4H_8$: Cl 35.69, H 4.03, O 32.19, Fe 28.09; found: Cl 35.66, H 4.06, O 32.19, Fe 28.09.

Synthesis of $[{^{57}Fe_{0.20}}^{56}Fe_{0.8}(bt)(NCS)_2]_2bpym]$: The synthesis was carried out under an argon atmosphere. A solution of KNCS (0.5 mmol) in methanol (15 mL) was added to a mixture of solutions of $FeCl_2·4H_2O$ (0.20 mmol) in methanol (15 mL) and $^{57}FeCl_2·4H_2O$ (0.05 mmol) in methanol (5 mL). The solution was stirred for 15 min and the resulting precipitate (KCl) was filtered off. The colourless solution containing Fe/NCS^- (1:2) was mixed with a solution of bt (0.25 mmol) in methanol (25 mL), changing the colour of the solution to violet. A solution of bpym (0.125 mmol) dissolved in methanol (15 mL) was added dropwise to this solution. The final dark red solution was filtered and allowed to evaporate for a week, giving a microcrystalline black-violet powder of **1**, 20% enriched with ^{57}Fe. Yield: 50%; elemental analysis calcd (%) for $C_{24}H_{14}N_{12}S_8Fe_2$: C 34.37, H 1.68, N 20.04; found: C 33.89, H 1.54, N 20.87.

Synthesis of $[{Zn_{0.85}Fe_{0.15}(bt)(NCS)_2}_2bpym]$ (2): The synthesis was carried out under an argon atmosphere. A solution of the bpym ligand (0.075 mmol) in methanol (10 mL) was added dropwise to a solution of $FeCl_2·4H_2O$ (0.15 mmol) in methanol (15 mL). The bt ligand (0.15 mmol) in methanol (15 mL) and subsequently KNCS (0.3 mmol) dissolved in methanol (10 mL) were added to this red solution. The final dark violet solution was filtered and kept under argon. The bpym ligand (0.425 mmol) dissolved in methanol (10 mL) was added dropwise to a solution of $ZnCl_2·4H_2O$ (0.85 mmol) in methanol (25 mL). The bt ligand (0.425 mmol) in methanol (15 mL) and subsequently KNCS (1.7 mmol) in methanol (10 mL) were added to this colourless solution. The colourless solution was filtered and mixed with the solution containing the iron complex. The resulting dark violet solution was stirred for 20 min and allowed to evaporate under argon for a week, giving a microcrystalline black-violet powder of **2**. Yield: 70%; elemental analysis calcd (%) for $C_{24}H_{14}N_{12}S_8Fe_{0.15}Zn_{0.85}$: C 33.68, H 1.63, N 19.64; found: C 33.49, H 1.62, N 19.57; the energy-dispersive X-ray microanalysis (EDXA) shows the presence of Fe and Zn, 14.47% and 85.53%, respectively.

Magnetic susceptibility measurements: The variable-temperature magnetic susceptibility measurements were performed on small single crystals using a Quantum Design MPMS2 SQUID susceptometer equipped with a 5.5 T magnet and operating at 1 T and 1.8–375 K. Experimental data were corrected for diamagnetism using Pascal's constants.

X-ray crystallographic study: Diffraction data for **1** at 293 K was collected with a Nonius Kappa-CCD single crystal diffractometer using $Mo_{K\alpha}$ radiation ($\lambda = 0.71073$ Å). A multiscan absorption correction was found to have no significant effect on the refinement results. The structures were solved by direct methods using SHELXS-97 and refined by full-matrix least-squares on F^2 using SHELXL-97.[21] All non-hydrogen atoms were refined anisotropically. The single-crystal X-ray diffraction experiments on **1** at 240, 175 and 30 K were carried out by using graphite monochromated $Mo_{K\alpha}$ radiation ($\lambda = 0.71073$ Å) on a Bruker SMART 1 K area detector diffractometer, equipped with a Cryostream N_2 open-flow cooling device[22] and an Oxford Cryosystems HeliX[23] (to obtain data at 30 K). In each case, a series of narrow ω-scans (0.3°) were performed at several ϕ settings in such a way as to cover a sphere of data to a maximum resolution of between 0.70 and 0.77 Å. Cell parameters were determined and refined using the SMART software,[24] and raw frame data were integrated using the SAINT program.[25] All structures were solved

by direct methods and refined by full-matrix least-squares on F^2 using SHELXTL software.[26] Reflection intensities were corrected by the multi-scan method, based on multiple scans of identical and Laue equivalent reflections (using the SADABS software).[27] All non-hydrogen atoms were refined with anisotropic displacement parameters. Although the hydrogen atoms were visible in the difference map, refinement of hydrogen positions led to an unreliable model, so they were positioned geometrically and refined using a riding model. CCDC-604837–CCDC-604840 contain the supplementary crystallographic data for this paper. These data can be obtained free of charge from The Cambridge Crystallographic Data Centre via www.ccdc.cam.ac.uk/data_request/cif.

Mössbauer spectroscopy: ^{57}Fe Mössbauer spectra were recorded by using a constant acceleration conventional spectrometer and helium bath cryostat. A superconducting magnet was used to create a magnetic field directed parallel to the wave vector of γ-quanta. The sample and the Mössbauer source $^{57}Co/Rh$ (Cyclotron) were immersed in liquid helium. About 40 mg of microcrystalline powder was placed in a 16 mm diameter absorber holder made of polished transparent acryl. The Recoil 1.03a Mössbauer Analysis Software was used to fit the experimental spectra. LIESST experiments were carried out using an Ar^+ laser (514 nm, 25 mW cm^{-2}, Coherent Innova 70).

[1] S. A. Wolf, D. D. Awschalom, R. A. Buhrman, J. M. Daughton, S. von Molnár, M. L. Roukes, A. Y. Chtchelkanova, D. M. Treger, *Science* **2001**, *294*, 1488–1495.

[2] a) "Spin Crossover in Transition Metal Compounds": , *Top. Curr. Chem.* **2004**, *233–235*, all three volumes; b) J. A. Real, A. B. Gaspar, M. C. Muñoz, *Dalton Trans.* **2005**, 2062–2079; c) J. A. Real, A. B. Gaspar, V. Niel, M. C. Muñoz, *Coord. Chem. Rev.* **2003**, *236*, 121–141; d) P. Gütlich, A. Hauser, H. Spiering, *Angew. Chem.* **1994**, *106*, 2109–2139; *Angew. Chem. Int. Ed. Engl.* **1994**, *33*, 2024–2054.

[3] a) A. Galet, A. B. Gaspar, M. C. Muñoz, G. V. Bukin, G. Levchenko, J. A. Real, *Adv. Mater.* **2005**, *17*, 2949–2953; b) O. Kahn, C. J. Martinez, *Science* **1998**, *279*, 44–48; c) O. Kahn, J. Kröber, C. Jay, *Adv. Mater.* **1992**, *4*, 718–728; d) Y. García, V. Ksenofontov, P. Gütlich, *Hyperfine Interact.* **2002**, *139/140*, 543–551.

[4] a) P. Gütlich, Y. Garcia, T. Woike, *Coord. Chem. Rev.* **2001**, *219–221*, 839–879; b) W. Sander, G. Bucher, F. Reichel, D. Cremer, *J. Am. Chem. Soc.* **1991**, *113*, 5311–5322; c) L. C. Bush, R. B. Heath, J. A. Berson, *J. Am. Chem. Soc.* **1993**, *115*, 9830–9831; d) K. Hamachi, K. Matsuda, T. Itoh, H. Iwamura, *Bull. Chem. Soc. Jpn.* **1998**, *71*, 2937–2943; e) K. Matsuda, M. Irie, *J. Am. Chem. Soc.* **2000**, *122*, 7195–7201; f) I. Ratera, D. Ruiz-Molina, J. A. Vidal-Gancedo, J. J. Novoa, K. Wurst, J.-F. Létard, C. Rovira, J. Veciana, *Chem. Eur. J.* **2004**, *10*, 603–616.

[5] a) M. Verdaguer, *Science* **1996**, *272*, 698–699; b) O. Sato, T. Iyoda, A. Fujishima, K. Hashimoto, *Science* **1996**, *272*, 704–705; c) V. Ksenofontov, G. Levchenko, S. Reiman, P. Gütlich, A. Bleuzen, V. Escax, M. Verdaguer, *Phys. Rev. B* **2003**, *68*, 024415 (1–6).

[6] a) J. A. Real, A. B. Gaspar, M. C. Muñoz, P. Gütlich, V. Ksenofontov, H. Spiering, *Top. Curr. Chem.* **2004**, *233*, 167–193; b) A. B.

Gaspar, V. Ksenofontov, V. Martínez, M. C. Muñoz, J. A. Real, P. Gütlich, *Eur. J. Inorg. Chem.* **2004**, 4770–4773; c) V. Ksenofontov, A. B. Gaspar, S. Reiman, N. Niel, J. A. Real, P. Gütlich, *Chem. Eur. J.* **2004**, *10*, 1291–1298; d) A. B. Gaspar, V. Ksenofontov, H. Spiering, S. Reiman, J. A. Real, P. Gütlich, *Hyperfine Interact.* **2002**, *144/145*, 297–306; e) V. Ksenofontov, A. B. Gaspar, J. A. Real, P. Gütlich, *J. Phys. Chem. B* **2001**, *105*, 12266–12271; f) V. Ksenofontov, H. Spiering, S. Reiman, Y. Garcia, A. B. Gaspar, N. Moliner, J. A. Real, P. Gütlich, *Chem. Phys. Lett.* **2001**, *348*, 381–386; g) V. Ksenofontov, H. Spiering, S. Reiman, Y. Garcia, A. B. Gaspar, N. Moliner, J. A. Real, P. Gütlich, *Hyperfine Interact.* **2002**, *141/142*, 47–52; h) G. Chastanet, A. B. Gaspar, J. A. Real, J-F. Létard, *Chem. Commun.* **2001**, 819–820; i) J-F Létard, J. A. Real, N. Moliner, A. B. Gaspar, L. Capes, O. Cador, O. Kahn, *J. Am. Chem. Soc.* **1999**, *121*, 10630–10631; j) J. A. Real, H. Bolvin, A. Bousseksou, A. Dworkin, O. Kahn, F. Varret, J. J. Zarembowitch, *J. Am. Chem. Soc.* **1992**, *114*, 4650–4658.

[7] N. O. Moussa, G. Molnár, S. Bonhommeau, A. Zwick, S. Mouri, K. Tanaka, J. A. Real, A. Bousseksou, *Phys. Rev. Lett.* **2005**, *94*, 107205 (1–4).

[8] A. B. Gaspar, V. Ksenofontov, J. A. Real, P. Gütlich, *Chem. Phys. Lett.* **2003**, *373*, 385–391.

[9] B. A. Leita, B. Moubaraki, K. S. Murray, J. P. Smith, J. D. Cashion, *Chem. Commun.* **2004**, 156–157.

[10] M. H. Klingele, B. Moubaraki, J. D. Cashion, K. S. Murray, S. Brooker, *Chem. Commun.* **2005**, 987–989.

[11] K. Nakano, N. Suemura, S. Kawata, A. Fuyuhiro, T. Yagi, S. Nasu, S. Morimoto, S. Kaizaki, *Dalton Trans.* **2004**, 982–988.

[12] K. Nakano, S. Kawata, K. Yoneda, A. Fuyuhiro, T. Yagi, S. Nasu, S. Morimoto, S. Kaizaki, *Chem. Commun.* **2004**, 2892–2893.

[13] N. Ortega-Villar, A. L. Thompson, M. C. Muñoz, V. M. Ugalde-Saldívar, A. E. Goeta, R. Moreno-Esparza, J. A. Real, *Chem. Eur. J.* **2005**, *11*, 5721-5734.

[14] S. R. Batten, J. Bjernemose, P. Jensen, B. A. Leita, K. S. Murray, B. Moubaraki, J. P. Smith, H. Toftlund, *Dalton Trans.* **2004**, 3370–3375.

[15] a) H. Koeppen, E. W. Müller, C. P. Köhler, H. Spiering, E. Meissner, P. Gütlich. Chem. Phys. Lett. **1982**, *91*, 348; b) D. Chernyshov, M. Hostettler, K. W. Törnoos, H. B. Bürgi, *Angew. Chem.* **2003**, *115*, 3955–3960; *Angew. Chem. Int. Ed.* **2003**, *42*, 3825–3830; c) C. M. Grunert, J. Schweifer, P. Weiberger, W. Linert, K. Mereiter, G. Hilscher, M. Müller, G. Wiesinger, P. J. Koningsbruggen, *Inorg. Chem.* **2004**, *43*, 155–165.

[16] a) V. Niel, A. L. Thompson, A. E. Goeta, C. Enachescu, A. Hauser, A. Galet, M. C. Muñoz, J. A. Real, *Chem. Eur. J.* **2005**, *11*, 2047–2060; b) M. Yamada, M. Ooidemizu, Y. Ikuta, S. Osa, N. Matsumoto, S. Iijima, M. Kojima, F. Dahan, J. P. Tuchages, *Inorg. Chem.* **2003**, *42*, 8406–8416.

[17] A. Ozarowski, B. R. McGarvey, A. B. Sarkar, J. E. Drake, *Inorg. Chem.* **1988**, *27*, 628–635.

[18] S. Zein, S. A. Borshch, *J. Am. Chem. Soc.* **2005**, *127*, 16197–16201.

[19] P. Gütlich, H. A. Goodwin, *Top. Curr. Chem.* **2004**, *233*, 1–48.

[20] A. Hauser, *Top. Curr. Chem.* **2004**, *234*, 155–198.

[21] G. M. Sheldrick, SHELX97, Program for Crystal Structure Determination, University of Gottingen, Germany, **1997**.

[22] J. Cosier, A. M. Glazer, *J. Appl. Crystallogr.* **1986**, *19*, 105.

[23] A. E. Goeta, L. K. Thompson, C. L. Sheppard, S. S. Tandon, C. W. Lehmann, J. Cosier, C. Webster, J. A. K. Howard, *Acta Crystallogr. Sect. C* **1999**, *55*, 1243–1246.

[24] SMART-NT, Data Collection Software, version 5.0, Bruker Analytical X-ray Instruments Inc.: Madison, Wisconsin, U. S. A., 1999.

[25] SAINT-NT, Data Reduction Software, version 5.0, Bruker Analytical X-ray Instruments Inc.: Madison, Wisconsin, USA, **1999**.

[26] SHELXTL, version 5.1, Bruker Analytical X-ray Instruments Inc., Madison, Wisconsin, USA, **1999**.

[27] G. M. Sheldrick, SADABS, Empirical Absorption Correction Program, University of Göttingen, Göttingen (Germany), **1998**.